

## Phase Diagram of Star Polymer Solutions

M. Watzlawek,<sup>1,\*</sup> C. N. Likos,<sup>1,2</sup> and H. Löwen<sup>1,2</sup>

<sup>1</sup>*Institut für Theoretische Physik II, Heinrich-Heine-Universität, Universitätsstraße 1, D-40225 Düsseldorf, Germany*

<sup>2</sup>*IFF Theorie II, Forschungszentrum Jülich GmbH, D-52425 Jülich, Germany*

(Received 13 January 1999)

The phase diagram of star polymer solutions in a good solvent is obtained over a wide range of densities and arm numbers by Monte Carlo simulations. The effective interaction between the stars is modeled by an ultrasoft pair potential which is logarithmic in the core-core distance. Among the stable phases are a fluid as well as body-centered cubic, face-centered cubic, body-centered orthogonal, and diamond crystals. In a limited range of arm numbers, reentrant melting and reentrant freezing transitions occur for increasing density. [S0031-9007(99)09465-X]

PACS numbers: 64.70.-p, 61.25.Hq, 82.70.Dd

A major challenge in statistical physics is to understand and predict the macroscopic phase behavior from a microscopic many-body theory for a given interaction between the particles [1]. For a simple classical fluid [2], this interaction is specified in terms of a radially symmetric pair potential  $V(r)$  where  $r$  is the particle separation. Significant progress has been made during the last decades in predicting the thermodynamically stable phases for simple intermolecular pair potentials, such as for Lennard-Jones systems, plasmas or hard spheres, using computer simulations [1], and density functional theory [3]. Important realizations of classical many-body systems are suspensions of colloidal particles dispersed in a fluid medium. A striking advantage of such colloidal samples over molecular ones is that their effective pair interaction is eminently tunable through experimental control of particle and solvent properties [4]. This brings about more extreme pair interactions, leading to novel phase transformations. For instance, if the colloidal particles are sterically stabilized against coagulation, the “softness” of the interparticle repulsion is governed by the length of the polymer chains grafted onto the colloidal surface, their surface grafting density, and solvent quality. Computer simulations and theory have revealed that a fluid freezes into a body-centered-cubic (bcc) crystal for soft long-ranged repulsions and into a face-centered-cubic (fcc) one for strong short-ranged repulsions [5]. This was confirmed in experiments on sterically stabilized colloidal particles [6]. A similar behavior occurs for charge-stabilized suspensions where the softness of  $V(r)$  is now controlled by the concentration of added salt [7]. Less common effects were observed for potentials involving an attractive part aside from a repulsive core. In reducing the range of the attraction, a vanishing liquid phase has been observed [8] and an isostructural solid-solid transition was predicted [9]. More complicated pair potentials can even lead to stable quasicrystalline phases and a quadruple point in the phase diagram [10].

The aim of this Letter is to study the phase diagram of an *ultrasoft* repulsive pair potential  $V(r)$  which is logarithmic in  $r$  inside a core of diameter  $\sigma$  and vanishes exponen-

tially in  $r$  outside the core. The motivation to do this is twofold: first, such a potential is a good model for the effective interaction between star polymers in a good solvent [11,12], which can be regarded as sterically stabilized particles where the size of the particles is much smaller than the length of the grafted polymer chains [13]. These stars are characterized by their arm number (or functionality)  $f$ , i.e., the number of polymer chains tethered to the central particle, and their corona diameter  $\sigma$  which measures the spatial extension of the monomer density around a single star center. Second, more fundamentally, phase transitions for such soft potentials are expected to be rather different from that for stronger repulsions. From a study of the pure logarithmic potential in two spatial dimensions [14], it is known that one needs a critical prefactor to freeze the system, which is quite different from, e.g., inverse-power potentials. Furthermore, the potential crossover at  $r = \sigma$  is expected to influence drastically the freezing transition, if the number density  $\rho$  of the stars is near the overlap concentration,  $\rho^* \approx 1/\sigma^3$ .

We obtain the full phase diagram of star polymer solutions by Monte Carlo simulation and theory. As a result, among the stable phases are a fluid as well as bcc, fcc, body-centered orthogonal (bco), and diamond crystals. We emphasize that the stability of a bco crystal with anisotropic rectangular elementary cell and a diamond structure was never obtained before for a *radially symmetric* pair potential. In fact, there is a widespread belief in the literature that anisotropic or three-body forces are solely responsible for a stable diamond lattice [15]. We show that both the crossover at  $r = \sigma$  and the ultrasoftness of the core are crucial for the stability of the bco and the diamond phase. Moreover, we get reentrant melting for  $34 \leq f \leq 60$ , and reentrant freezing for  $44 \leq f \leq 60$  as  $\rho$  is increasing. Some features of the presented phase diagram have already been observed in a system of copolymer micelles exhibiting a very similar interaction to star polymers [6,16].

With  $k_B T$  denoting the thermal energy, our effective pair potential between two star centers is a combination of a logarithm inside the core of size  $\sigma$  and a Yukawa potential

outside the core [12],

$$V(r) = \frac{5}{18} k_B T f^{3/2} \begin{cases} -\ln\left(\frac{r}{\sigma}\right) + \frac{1}{1+\sqrt{f}/2} & (r \leq \sigma), \\ \frac{\sigma}{1+\sqrt{f}/2} \frac{\exp[-\sqrt{f}(r-\sigma)/2\sigma]}{r} & (r > \sigma), \end{cases} \quad (1)$$

such that both the potential and its first derivative (or, equivalently, the force) are continuous at  $r = \sigma$  [12]. The decay length of the exponential is given by the largest blob diameter within the Daoud-Cotton theory for single star polymers [17]. Experimental support for this potential comes from neutron scattering data on the structural ordering of 18-arm stars in the fluid phase [12] and shear moduli measurements in the crystalline phase of micelles [18]. Furthermore, microscopic simulations of two star polymers have shown that this potential provides an excellent description of the effective star interaction for a broad range of arm numbers [19]. We note that  $V(r)$  becomes the hard sphere potential for  $f \rightarrow \infty$ .

Because of the purely entropic origin of the interstar repulsion, the strength of the pair potential (1) scales linearly with  $k_B T$ , causing the temperature to be an irrelevant thermodynamic quantity. Therefore, for the calculation of the phase diagram, only the packing fraction of the stars,  $\eta = \pi/6\rho\sigma^3$ , and the arm number  $f$  matter, the latter playing the role of an “effective inverse temperature.” We use computer simulations to access the phase diagram. The free energies of the fluid phase and several possible solid phases are calculated by thermodynamic integration via Monte Carlo simulations [20]. The free energy of the fluid phase,  $F_{fl}$ , is obtained either by the well-known “pressure or density route” [2,20], or, alternatively, by the so-called “ $f$  route.” The pressure route relates the free energy for nonvanishing  $\eta$  to that at zero packing fraction, keeping  $f$  fixed. In the  $f$  route,  $f$  is used as an artificial thermodynamic variable, now keeping  $\eta$  fixed. The free energy of star polymers with a certain arm number  $f$  is then obtained by the following integration:

$$F_{fl} = \int_0^f df' \left\langle \frac{\partial U}{\partial f'} \right\rangle_{f'}. \quad (2)$$

Here,  $U = \sum_{i<j} V(|\mathbf{r}_i - \mathbf{r}_j|)$  is the total potential energy function which depends on  $f$  since  $V(r)$  depends on  $f$  parametrically.  $\langle \dots \rangle_{f'}$  denotes the canonical ensemble average for a system with fixed arm number  $f'$ . Therefore, in order to carry out the  $f$ -route integration, a series of simulations at fixed  $\eta$  but for increasing  $f'$  is performed to calculate the integrand of Eq. (2).

We use the Frenkel-Ladd method for continuous potentials to obtain the free energy of the solid phases [20,21]. For these Monte Carlo calculations, suitable candidate crystal structures have to be chosen. Our method to get information about the possible stable structures for fixed

$f$  and  $\eta$  consists of two steps: first, we calculate lattice sums for a wide class of crystals, including the “usual” structures with cubic elementary cells (fcc, bcc, hcp, and simple cubic) and several “unusual” structures. These unusual structures are the hexagonal lattice, the diamond lattice, representations of quasicrystalline structures (see, e.g., Ref. [10]), and generalizations of the usual structures, which were obtained by stretching the elementary cell lengths (denoted as  $a$ ,  $b$ , and  $c$ ) of these structures by arbitrary factors, then using the two independent ratios  $b/a$  and  $c/a$  as minimization parameters of the lattice sum. Second, we calculate the global bond order parameters [22] of the equilibrated structures, which were spontaneously formed in a first set of simulations, always starting from a purely random configuration. Crystal structures whose bond order parameters are in agreement with these measured parameters, and which have reasonably small values of the lattice sum, are then chosen as candidate structures for the free energy calculations. This procedure was performed for a wide range of arm numbers  $18 \leq f \leq 512$  and packing fractions  $0 \leq \eta \leq 1.5$ . Finally, the obtained free energy data at fixed  $f$  were used to explore the phase boundaries via the common double tangent construction. The resulting phase diagram is displayed in Fig. 1. In the explored range of  $f$  and  $\eta$ , four different stable crystal structures are found besides a fluid phase. For  $f < f_c \approx 34$ , the fluid phase is stable for all densities, which is in agreement with results obtained from an effective hard sphere mapping procedure [23] and from scaling theory [11]. We remark that Witten *et al.* [11] only estimated  $f_c$  within 1 order of magnitude to be around  $f \approx 100$ . For  $f \geq f_c$ , at least one stable

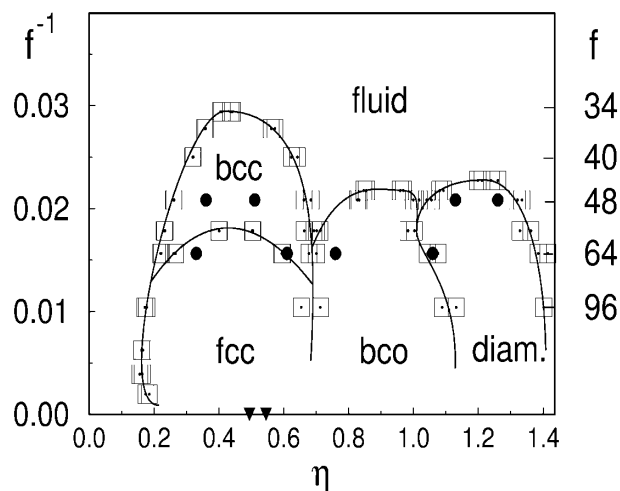


FIG. 1. The phase diagram of star polymer solutions for different arm numbers  $f$  versus packing fraction  $\eta$ . The squares and the circles indicate the phase boundaries as obtained from computer simulations and theory, respectively; lines are only guides to the eye. The statistical error of the simulations is of the order of the symbol size. The triangles indicate the freezing and melting point of hard spheres.

crystal phase is found. We focus first on the crystal phases at  $0.2 \lesssim \eta \lesssim 0.7$ : for  $f_c < f \lesssim 54$ , a bcc phase is found, whereas for  $f \gtrsim 70$ , only the fcc structure turns out to be stable. At intermediate  $f$  ( $54 \lesssim f \lesssim 70$ ), bcc-fcc phase transitions occur. For  $0.2 \lesssim \eta \lesssim 0.7$ , the mean interparticle distance  $\bar{r} = \rho^{-1/3}$  is larger than  $\sigma$ , leaving only the exponential part of  $V(r)$  to be relevant for the phase behavior. Therefore, the observance of a fcc phase for large  $f$ , corresponding to a short-range, strongly screened potential, and a bcc phase for small  $f$ , corresponding to a long-range, less screened potential, is analogous to the phase behavior found for charged colloids [5,7]. In Fig. 1, the freezing and melting points for hard spheres, corresponding to  $f \rightarrow \infty$ , are shown as well, denoted by black triangles. We emphasize that even star polymers with very high arm numbers freeze at considerably smaller  $\eta$  than hard spheres. In fact, our simulations show that a “hard sphere-like” structure is found only for extremely high arm numbers  $f \gtrsim 10\,000$ . Thus the change in the phase boundary cannot be shown on the scale of the figure.

Let us now consider the phase behavior for  $\eta \approx 0.7$ , where  $\bar{r}$  is in the order of  $\sigma$  and the logarithmic part of  $V(r)$  becomes relevant. From our calculations, a reentrant melting transition, i.e., a transition from a solid to a liquid phase with increasing  $\eta$ , is found for  $34 < f \lesssim 60$ . We note that this reentrant melting was already predicted qualitatively by Witten *et al.* [11]. For  $f \gtrsim 60$ , a solid-solid phase transformation into a bco phase takes place. This unusual phase is stable up to  $\eta \approx 1.0$ . For  $44 \lesssim f \lesssim 60$ , the remolten liquid refreezes into this bco structure at  $\eta \approx 0.80$ . At  $\eta \approx 1.0$ , a further solid-solid phase transition from the bco into a diamond structure is found, the latter being stable for arm numbers  $f \gtrsim 44$  and packing fractions up to  $\eta \approx 1.4$ – $1.5$ . Notice that the extension of the two phase regions (“density jumps”) of all encountered phase transitions is extremely small due to the soft character of  $V(r)$  [24]. Moreover, the empirical Hansen-Verlet freezing rule [25] is valid for *all* points at the phase boundaries where we calculated the static structure factor  $S(q)$ . This also includes the reentrant melting transition for  $\eta \approx 0.7$ , where the  $S(q)$  for the fluid begins to show unusual behavior [23].

We develop now a physical intuition for the unusual occurrence of the bco and diamond phase. For this purpose, we report first on the detailed structure of the bco phase. At fixed  $\eta$ , the bco crystal is described by the two length ratios of its elementary cell,  $b/a$  and  $c/a$ , respectively. In order to calculate the free energy of the bco crystal by the Frenkel-Ladd method, these ratios had to be determined from a first set of simulations. In these  $NpT$  simulations [20], the system was free to adopt its optimal values for  $b/a$  and  $c/a$ , starting either from a purely random configuration or an initial bco configuration. Within the error bars, the so determined elementary cell length ratios were in agreement with the values obtained from the minimization of the lattice sums. We therefore took the lattice sum

results as input for the free energy calculations. These ratios increase with  $\eta$  from  $b/a \approx 2.24$  and  $c/a \approx 1.32$  at  $\eta = 0.7$  to  $b/a \approx 3.14$  and  $c/a \approx 1.81$  at  $\eta = 1.0$  and are nearly independent of  $f$ . Figure 2 illustrates the resulting structure. As can be seen from this figure, the anisotropy of the elementary cell leads to a strong interpenetration of the particle coronas along one of the lattice axes. In fact, over the whole stability range of the bco phase, the next neighbor distance along this axis is considerably smaller than  $\sigma$ , whereas all other next neighbor distances are larger than  $\sigma$ . This can be intuitively understood from the form of the potential (1): because of the weak divergence for small  $r$ , there is no huge energy penalty in bringing the nearest neighbors close together. On the other hand, the potential falls off rapidly for  $r > \sigma$ , so all the remaining neighbor shells are not costly in energy, too. With increasing  $\eta$ , the distance of the two nearest neighbors in the bco is decreasing until the energy

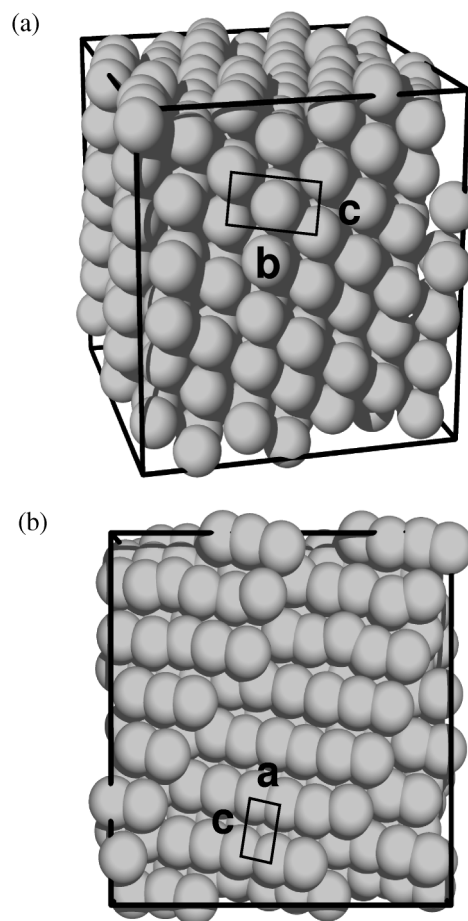


FIG. 2. (a) A snapshot of a typical bco configuration for  $f = 64$  and  $\eta = 0.8$  in a periodically repeated (cubic) simulation box. The diameter of the spheres is the corona diameter  $\sigma$ ; (b) Same as (a), now seen from the “left” side of the simulation box shown in (a). Notice the high anisotropy of the lattice spacings. The elementary cell length ratios are  $b/a \approx 2.70$  and  $c/a \approx 1.57$ .

penalty becomes significant. Hence, the bco will then lose against another structure with more than two nearest neighbors inside the corona. A suitable structure is the diamond phase which possesses four tetrahedrally ordered nearest neighbors. Indeed, our simulations show that all the other neighbors are kept outside the corona in the stability range of the diamond. Therefore, both the ultrasoft logarithmic part and the crossover at  $r = \sigma$  are crucial for the stability of the bco and the diamond phase. This provides a simple reason why such phases have not been found earlier for strongly repulsive interactions. We further note that the presented scenario also nicely expresses itself in the angle-average radial distribution functions  $g(r)$  of the bco and diamond solid, which show a similar anomaly as found in the  $g(r)$  of the fluid phase [23].

As for a further theoretical investigation, we solved the accurate Rogers-Young closure [26] to obtain the free energy of the fluid for  $f = 18, 32, 40, 48,$  and  $64$ . For the aforementioned solid structures, we used the Einstein-crystal perturbation theory [27] to calculate the associated free energies. As this theory provides only an *upper bound* to the free energy, the domain of stability of the fluid is enhanced in comparison to the simulation results. The theory predicts  $40 < f_c < 48$  and eliminates the domain of stability of the bcc crystal. Otherwise, as also shown in Fig. 1, the same phase behavior as determined from simulations emerges.

We finally note that all our predictions for  $\rho \leq 2\rho^*$ , i.e.,  $\eta \lesssim 1.0$ , should be verifiable in scattering experiments, since for these densities pair interactions are dominant. In fact, in recent experimental work on spherical diblock copolymer micelles, Gast and co-workers have already confirmed a part of our results [6,16]. The freezing transition in fcc and bcc crystals depending on the number of arms  $f$  is found [6] as well as reentrant melting with increasing  $\eta$  [16]. For the “most starlike” system, also a reentrant freezing is observed as predicted in Fig. 1. For  $\eta \gtrsim 1.0$  however, when three stars exhibit overlaps within their coronae, many body interactions become important, which we have neglected in our calculations using the pair potential (1). Nevertheless, from a theoretical point of view, this potential turned out to be interesting also for  $\eta \gtrsim 1.0$ , resulting for the first time in a stable diamond structure for a purely radially symmetric pair interaction.

In conclusion, we have determined the phase diagram of star polymers over a broad range of arm numbers  $f$  and packing fractions  $\eta$  by computer simulations and theory. The phase diagram includes a fluid phase as well as four stable crystal phases. These crystal phases are a fcc crystal and a bcc crystal, as well as an unusual anisotropic bco structure and a diamond crystal.

It is a pleasure to thank Professor Daan Frenkel for helpful remarks. We further thank the Deutsche Forschungsgemeinschaft for support within SFB 237.

\*Corresponding author.

Email address: martin@thphy.uni-duesseldorf.de

- [1] *Observation, Prediction and Simulation of Phase Transitions in Complex Fluids*, edited by M. Baus, L.F. Rull, and J.P. Ryckaert (Kluwer, Dordrecht, The Netherlands, 1995).
- [2] See, e.g., J.P. Hansen and I.R. McDonald, *Theory of Simple Liquids* (Academic, New York, 1986), 2nd ed.
- [3] H. Löwen, Phys. Rep. **237**, 249 (1994).
- [4] P.N. Pusey, in *Liquids, Freezing and the Glass Transition*, edited by J.P. Hansen, D. Levesque, and J. Zinn-Justin (North-Holland, Amsterdam, 1991).
- [5] M.O. Robbins, K. Kremer, and G.S. Grest, J. Chem. Phys. **88**, 3286 (1988); W.G. Hoover, S.G. Gray, and K.W. Johnson, J. Chem. Phys. **55**, 1128 (1971); J.F. Lutsko and M. Baus, J. Phys. Condens. Matter **3**, 6547 (1991).
- [6] G.A. McConnell *et al.*, Phys. Rev. Lett. **71**, 2102 (1993).
- [7] E.B. Sirota *et al.*, Phys. Rev. Lett. **62**, 1524 (1989).
- [8] S.M. Ilett *et al.*, Phys. Rev. E **51**, 1344 (1995).
- [9] P. Bolhuis and D. Frenkel, Phys. Rev. Lett. **72**, 2211 (1994).
- [10] A.R. Denton and H. Löwen, Phys. Rev. Lett. **81**, 469 (1998); Prog. Colloid Polym. Sci. **104**, 160 (1997).
- [11] T.A. Witten, P.A. Pincus, and M.E. Cates, Europhys. Lett. **2**, 137 (1986); T.A. Witten and P.A. Pincus, Macromolecules **19**, 2509 (1986).
- [12] C.N. Likos *et al.*, Phys. Rev. Lett. **80**, 4450 (1998).
- [13] G.S. Grest *et al.*, Adv. Chem. Phys. **XCIV**, 67 (1996).
- [14] J.P. Hansen and D. Levesque, J. Phys. C **14**, 1603 (1981); J.M. Caillol *et al.*, J. Stat. Phys. **28**, 325 (1982).
- [15] F.H. Stillinger and T.A. Weber, Phys. Rev. B **31**, 5262 (1985); R. Biswas and D.R. Hamann, Phys. Rev. Lett. **55**, 2001 (1985); J. Tersoff, Phys. Rev. Lett. **56**, 632 (1985); S.R. Phillipot *et al.*, Phys. Rev. B **40**, 2831 (1989).
- [16] G.A. McConnell and A.P. Gast, Macromolecules **30**, 435 (1997).
- [17] M. Daoud and J.P. Cotton, J. Phys. (Paris) **43**, 531 (1982).
- [18] J. Buitenhuis and S. Förster, J. Chem. Phys. **107**, 262 (1997).
- [19] A. Jusufi, M. Watzlawek, and H. Löwen, Macromolecules (to be published).
- [20] D. Frenkel and B. Smit, *Understanding Molecular Simulation* (Academic, San Diego, 1996).
- [21] D. Frenkel, Phys. Rev. Lett. **56**, 858 (1986).
- [22] P.J. Steinhardt, D.R. Nelson, and M. Ronchetti, Phys. Rev. B **28**, 784 (1983); P.R. ten Wolde, M.J. Ruiz-Montero, and D. Frenkel, Phys. Rev. Lett. **75**, 2714 (1995).
- [23] M. Watzlawek, H. Löwen, and C.N. Likos, J. Phys. Condens. Matter **10**, 8189 (1998).
- [24] A consideration of the so-called “volume terms” would lead to even smaller density jumps; see, e.g., H. Graf and H. Löwen, Phys. Rev. E **57**, 5744 (1998).
- [25] J.P. Hansen and L. Verlet, Phys. Rev. **184**, 151 (1969).
- [26] F.J. Rogers and D.A. Young, Phys. Rev. A **30**, 999 (1984).
- [27] C.F. Tejero *et al.*, Phys. Rev. Lett. **73**, 752 (1994); Phys. Rev. E **51**, 558 (1995).